# Vibrational Spectra of a Mechanosensitive Channel

Chungwen Liang,[†] Martti Louhivuori,[‡] Siewert J. Marrink,[‡] Thomas L. C. Jansen,[*,†] and Jasper Knoester[†]

*Center for Theoretical Physics and Zernike Institute for Advanced Materials, University of Groningen, Nijenborgh 4, 9747 AG Groningen, The Netherlands, and Groningen Biomolecular Sciences and Biotechnology Institute, Nijenborgh 7, 9747 AG Groningen, The Netherlands*

E-mail: T.L.C.Jansen@rug.nl

[*]To whom correspondence should be addressed

[†]Center for Theoretical Physics and Zernike Institute for Advanced Materials, University of Groningen, Nijenborgh 4, 9747 AG Groningen, The Netherlands

[‡]Groningen Biomolecular Sciences and Biotechnology Institute, Nijenborgh 7, 9747 AG Groningen, The Netherlands

# Computational details

### All-atom Molecular Dynamics Simulation

All-atom MD simulations are performed using the GROMACS 4.5 package[1] with the GROMOS96 53a6 force field[2] for the proteins, the modified Berger's force field[3] for the lipids, and the SPC/E model[4] for the water molecules. The closed, intermediate (inter) and open states of the Tb-MscL are based on previous coarse-grained MD simulations[5]. The closed state corresponds to the crystal structure relaxed in the membrane environment. The intermediate state is characterized by tension induced expansion of the periplasmic side that however does not open the channel. In the open state the cytoplasmic side is also expanded, the hydrophobic lock is broken, and the channel is able to conduct water, ions, and small solutes. For a more detailed description of these states we refer to previous studies[5,6]. The atomistic structures are reconstructed from the corresponding coarse-grained representations using restrain-coupled simulated annealing MD in vacuum[7]. During the reconstruction, the protein is allowed to optimize its atomistic details while the system is cooling down. After that, the restraints to the underlying coarse-grained representation were gradually removed to ensure a smooth relaxation of the atomistic structure. Then, the atomistic channel is embedded inside a bilayer of 300 DOPC lipid molecules by using Kandt's method[8] and solvated with $\sim$ 16000 water ($D_2O$) molecules. After this a 2 ns of position restrained simulation on all protein atoms is performed followed by 2 ns position restrained simulation on the protein $C_\alpha$ atoms. Finally, after a 2 ns simulation without any restraint, the systems are assumed to be equilibrated and the 2 ns production runs are made.

During all simulations, the SETTLE algorithm[9] is used to constrain bond lengths and angles of the water molecules, and the LINCS algorithm[10] is used for all other bonds and angles, allowing an integration time step of 2 fs. Long-range electrostatic interactions are calculated by the Particle-Mesh-Ewald (PME) method[11] and short-range repulsive and attractive dispersion interactions are described with Lennard-Jones potentials, using 0.9 nm as cutoff length. The temperature of the

system is kept constant with the Nosé-Hoover coupling method[12,13] on the protein, lipids and water molecules (time constant $\tau$=0.1 ps) separately with an external heat bath at 310 K, in order to be consistent with the original parameterization conditions[3]. Similarly, the pressure is kept constant with semi-isotropic Parrinello-Rahman coupling[14] (time constant $\tau$=1 ps) separately to a pressure bath of 1 bar. The simulation time of each state is 2 ns.

**Infrared and SFG response Modeling**

We use the following form of the time-dependent Hamiltonian of amide I oscillators:

$$\begin{aligned} H(t) &= \sum_{i=1}^{N}\left[\omega_i(t)\mathbf{B}_i^{\dagger}\mathbf{B}_i - \frac{\Delta}{2}\mathbf{B}_i^{\dagger}\mathbf{B}_i^{\dagger}\mathbf{B}_i\mathbf{B}_i\right] + \sum_{i,j}^{N} J_{ij}(t)\mathbf{B}_i^{\dagger}\mathbf{B}_j \\ &+ \sum_{i=1}^{N}\vec{\mu}_i(t)\cdot\vec{E}(t)\left[\mathbf{B}_i^{\dagger}+\mathbf{B}_i\right] + \sum_{i=1}^{N}\alpha_i(t):\vec{E}^2(t)\left[\mathbf{B}_i^{\dagger}+\mathbf{B}_i\right] \end{aligned} \tag{1}$$

where $\mathbf{B}_i^{\dagger}$ and $\mathbf{B}_i$ are Bosonic creation and annihilation operators, respectively, of the $i$th oscillator. Furthermore, $\omega_i(t)$ is its vibrational frequency, and $J_{ij}(t)$ is the resonance coupling between the $i$th and the $j$th oscillators. $\vec{\mu}_i(t)$ and $\alpha_i(t)$ are the transition dipole and transition polarizability responsible for the coupling to the applied laser field $\vec{E}(t)$, respectively. $\Delta$ = 16 cm$^{-1}$ is the anharmonicity, which accounts for the fact that the energy gap between the single and double excited vibrational states is smaller than that between the ground state and the single excited state. The vibrational frequency is affected by the fluctuating local environment.

We consider two types of amino acid groups. For the secondary amide units, the frequency shifts and nearest neighbor couplings of the neighboring amide units in the peptide chain are accounted for with a dihedral map obtained from *ab initio* calculations on glycinedipeptide[15]. The frequency changes induced by the remaining environment is then determined with an electrostatic map based on N-methyl acetamide. This accounts for the effect of a local electric field and the electric field gradient[16]. For the 15 tertiary amide units found in Tb-MscL (i.e. those preceding proline in the backbone), the dihedral maps for nearest neighbor couplings and the frequency shifts due to nearest neighbors involving proline were used. These were calculated by a procedure similar

to that of the secondary amide groups using glycine-proline dipeptides for the parameterization[17]. For these groups an electrostatic map which accounts for the contribution of remaining environment based on *ab initio* calculations on N,N-dimethyl acetamide[17] were used. The side chain amide groups were not included in this study. These primary amide groups typically have amide I frequencies about 25 $cm^{-1}$ higher than the secondary amide units.[18] For both the secondary and tertiary amides, the non-nearest-neighbor couplings were calculated by using the transition charge coupling scheme[15,17]. This treatment is identical to that previously applied to Elastin like peptides[19] and very similar to the one recently benchmarked on parallel $\beta$-sheet amyloids.[20]

The amide I vibrational frequency of the $i$th site is modeled through:

$$\begin{aligned} \omega_i &= \omega_{gas} + \Delta\omega_N(\varphi_{i,i-1}, \psi_{i,i-1}) + \Delta\omega_C(\varphi_{i,i+1}, \psi_{i,i+1}) \\ &+ \Delta\omega_{map}(E(r), \nabla E(r)) \end{aligned} \tag{2}$$

where $\omega_{gas}$ is the gas phase frequency, $\Delta\omega_N$ is the frequency shift originating from the previous site $i$-1 toward the N terminus, while $\Delta\omega_C$ is the frequency shift originating from the next site $i$+1 toward the C terminus. $\varphi_{i,i\pm1}$ and $\psi_{i,i\pm1}$ are the dihedral angles between the $i$th and $(i\pm1)$th amide I groups. $\Delta\omega_{map}$ is the frequency shift due to the electric field generated by surrounding protein, lipid, and water molecules[16,17]. The transition dipole $\vec{\mu}_i(t)$ and transition polarizability $\alpha_i(t)$ fluctuate with the orientation of the $i$th amide I group, as well as with the local electric field $E(r)$ and electric field gradient $\nabla E(r)$[16,17]. The polarization of infrared spectra is obtained using the proper orientational averaging over different polarization directions[21].

The SFG process involves an infrared field $\vec{E}_k(\omega_{ir})$ (frequency $\omega_{ir}$, polarization direction $\hat{k}$), and a subsequent visible field $\vec{E}_j(\omega_{vis})$ (frequency $\omega_{vis}$, polarization direction $\hat{j}$). The second-order nonlinear polarization $\vec{P}_i^{(2)}(\omega_{SFG})$ (frequency $\omega_{SFG} = \omega_{ir} + \omega_{vis}$, polarization direction $\hat{i}$) is then generated by the applied fields $\vec{E}_k(\omega_{ir})$ and $\vec{E}_j(\omega_{vis})$ through the second-order nonlinear susceptibility $\chi_{ijk}^{(2)}$. It vanishes in the bulk of centrosymmetric materials, and thus also in isotropic

materials on average.

$$\vec{P}_i^{(2)}(\omega_{SFG}) = \varepsilon_0 \chi_{ijk}^{(2)}(\omega_{vis}, \omega_{ir}) \vec{E}_j(\omega_{vis}) \vec{E}_k(\omega_{ir}) \tag{3}$$

where the $\chi_{ijk}^{(2)}$ is a third rank tensor, whose 27 elements depend on the properties of the medium under investigation. At molecular interfaces, $\chi_{ijk}^{(2)}$ is reduced to seven non-vanishing elements by symmetry constraints. If an azimuthally isotropic polarization sheet in the *xy* plane is considered, there are only four independent elements remaining[22]:

$$\chi_{zzz}^{(2)}, \quad \chi_{xxz}^{(2)} = \chi_{yyz}^{(2)}, \quad \chi_{xzx}^{(2)} = \chi_{yzy}^{(2)}, \quad \chi_{zxx}^{(2)} = \chi_{zyy}^{(2)} \tag{4}$$

In a SFG experiment, these four independent elements contribute to the signal under four different lab frame polarization conditions: *ppp*, *ssp*, *sps*, and *pss*. Here, we will only consider the $\chi_{zzz}^{(2)}$ and $\chi_{xxz}^{(2)}$ polarizations which determine the outcome of the SFG *ppp* and *ssp* measurements[23–26], respectively.

For calculating the SFG response functions, the amide I transition polarizability tensor $\alpha_{ij}$ is needed. We use Tsuboi's tensor matrix $\alpha''$[27] which was determined for proteins with $\alpha$-helical structure, where the tilt angle (between the principal *x*-axis and the C=O bond) $\theta = 34^\circ$ (see Figure S1). Then, we transform it to the local molecular frame, where the $x'$-axis is along the C=O bond direction. Using the rotational transformation, we then get:

$$\alpha' = \mathbf{S}\, \alpha''\, \mathbf{S}^T \tag{5}$$

$$\alpha' = \begin{bmatrix} \cos\theta & -\sin\theta & 0 \\ \sin\theta & \cos\theta & 0 \\ 0 & 0 & 1 \end{bmatrix} \begin{bmatrix} 20 & 0 & 0 \\ 0 & 4 & 0 \\ 0 & 0 & 1 \end{bmatrix} \begin{bmatrix} \cos\theta & \sin\theta & 0 \\ -\sin\theta & \cos\theta & 0 \\ 0 & 0 & 1 \end{bmatrix} = \begin{bmatrix} \alpha_{xx} & \alpha_{xy} & 0 \\ \alpha_{yx} & \alpha_{yy} & 0 \\ 0 & 0 & \alpha_{zz} \end{bmatrix}$$

where $\alpha_{xx}$ = 15, $\alpha_{xy} = \alpha_{yx}$ = 9, $\alpha_{yy}$ = 7.4 and $\alpha_{zz}$ = 1. The tensor element is given in unit of zz tensor component for which the value was not determined by the experiment[27]. A similar

transformation is applied to the tensor matrix $\alpha'$ into the simulation box frame, where the z-axis is parallel to the membrane normal. The transition polarizability tensor in this frame is used to calculate the SFG response functions.

Using all-atom MD simulations, the local structure of the protein chains, lipids, and the surrounding solvent is known. Then, using the above mapping, the time-dependent Hamiltonian is constructed for all amide I units. From this Hamiltonian, FTIR, LDIR, 2DIR and SFG spectra are calculated by using the numerical integration of the Schrödinger equation (NISE) method[28]. This quantum-classical method is based on numerically solving the time-dependent Schrödinger equation for the vibrational Hamiltonian $H(t)$ and using the solution to calculate optical response functions. The Schrödinger equation for the time-dependent Hamiltonian is solved numerically by successive propagation during time intervals that are short enough for the Hamiltonian to be considered constant, i.e. shorter than the time scale of the frequency fluctuations. In practice, it turns out that time intervals of 20 fs are short enough for this purpose[28,29]. The time domain response functions governing the infrared and SFG signal are then calculated by averaging over multiple starting configurations. The frequency domain spectra are calculated as a Fourier transform of the time domain response functions.

**The average tilt angle**

The average tilt angle $\theta$ of the amide I transition dipole is estimated from the relationship between LDIR and FTIR spectra. Using $z$ as the unique axis in the LDIR experiment Assuming one fixed transition dipole the following relations

$$\begin{aligned} I_{FTIR}(\omega) &= I_{xx}(\omega)+I_{yy}(\omega)+I_{zz}(\omega) \\ I_{LDIR}(\omega) &= -I_{xx}(\omega)-I_{yy}(\omega)+I_{zz}(\omega) \end{aligned} \tag{6}$$

can be used to derive the following equation for the angle $\theta$ between the dipole vector and the membrane surface normal.

$$\theta(\omega) = \arccos\left[\frac{1}{3} + \frac{2}{3}\frac{I_{LDIR}(\omega)}{I_{FTIR}(\omega)}\right]^{\frac{1}{2}} \tag{7}$$

In reality, however, with many contributing transition dipoles fluctuating with time, $\theta$ is a highly convoluted quantity that nevertheless gives an idea of orientational changes.

# Analysis

### SFG response functions for Different Groups

To further understand the lineshape of the SFG response functions, we calculate the SFG response functions of individual groups as shown in Figure S2. The contribution from the S1 and Loop region is negligible, because the amide I transition dipoles of S1 helices and Loop region are mainly perpendicular to the membrane surface normal. The transmembrane helices TM1 and TM2 contribute strong positive and negative signals, respectively, because the amide I transition dipoles along TM1 helices are pointing to the positive direction of the membrane surface normal, where the amide I transition dipoles along TM2 helices are in the opposite direction. The S2 helices contribute slightly to the negative signal in the high frequency region because of their orientation. The separated TM2 SFG response of the intermediate state are redshifted and have a stronger negative signal than that of the closed and open state (Figure S4), which results in stronger negative signal of the overall SFG response of the intermediate state, because the cancellation with the positive TM1 signal is less pronounced at 1645 $cm^{-1}$ in the intermediate state.

### 2DIR Spectra for Different Groups

To understand the 2DIR lineshape, we calculated the 2DIR spectra with parallel and perpendicular polarization for different groups of the channel as shown in Figures S3 and S4, respectively. In

Figure S5 diagonal slices through these spectra are presented. No significant difference is found between the two polarization directions except for the parallel spectra being about three times more intense. For the TM1 helices, the peak is located at 1655 $cm^{-1}$ in the closed state and 1650 $cm^{-1}$ in the open state. In the intermediate state a strong peak at 1655 $cm^{-1}$ is observed and a weaker one at 1650 $cm^{-1}$ at the same time the spectrum in the intermediate state is broader than in the other states. For the TM2 helices, a sharp peak at 1650 $cm^{-1}$ is observed for all states. In the intermediate state this peak is slightly redshifted, narrower, and more intense than those in the closed and open states. These are signatures of a more ordered helix in the intermediate state.[30] In the S1 and S2 helices the spectra are broader and contain multiple sub peaks indicating disorder and a lack of perfect helical structure. For the loop region the spectra are broader and blue shifted compared to the other groups. This the the typical spectrum of a random coil like structure.[31] There is little difference in the loop region spectra for the three different states. The peaks of the TM1 and TM2 groups are about 20 $cm^{-1}$ lower than the average site frequency. This difference is due to the collective property of the eigenstates as also known from other studies.[32–34] There is also essentially no difference in the average site frequencies for TM1 and TM2, but still the observed peak positions are different, which can thus only come from differences in the couplings. Such effects may arise from interactions between the helices.[35] The average frequencies are slightly higher for the Loop and S1 than for TM1 and TM2.

**Tilt angle of transmembrane helices**

To compare the tilt angle of transmembrane helices $\theta_{helix}$ to the average tilt angle of amide I transition dipoles ($\theta$ in the main text), we calculated the angle between the principal axis of helix and the membrane surface normal shown in Table S1. This was done using the Gromacs g_helixorient tool. We found that the values of $\theta_{helix}$ are not equal to that of the average tilt angle of amide I transition dipoles at 1645 $cm^{-1}$ (manuscript Figure 2). However, the general trends are similar. Both transmembrane helices and amide I transition dipole tilt more in the open state than in the close and intermediate states.

## References


(1) Lindahl, E.; Hess, B.; van der Spoel, D. Gromacs 3.0: A Package for Molecular Simulation and Trajectory Analysis. *J. Mol. Mod.* **2001**, *7*, 306–317.

(2) Oostenbrink, C.; Villa, A.; Mark, A. E.; van Gunsteren, W. F. A Biomolecular Force Field Based on the Free Enthalpy of Hydration and Solvation: The GROMOS Force-Field Parameter Sets 53A5 and 53A6. *J. Comput. Chem* **2004**, *25*, 1656–1676.

(3) Siu, S.; Vacha, R.; Jungwirth, P.; Böckmann, R. A. Biomolecular Simulations of Membranes: Physical Properties from Different Force Fields. *J. Chem. Phys* **2008**, *28*, 125103.

(4) Berendsen, H. J. C.; Grigera, J. R.; Straatsma, T. P. The Missing Term in Effective Pair Potentials. *J. Phys. Chem* **1987**, *91*, 6269–6271.

(5) Louhivuori, M.; Risselada, H.; van der Giessen, E.; Marrink, S. Release of Content Through Mechano-sensitive Gates in Pressurized Liposomes. *Proc. Natl. Acad. Sci. USA* **2010**, *16*, 19856–19860.

(6) Ollila, O. H. S.; Louhivuori, M.; Marrink, S. J.; Vattulainen, I. Protein Shape Change has a Major Effect on the Gating Energy of a Mechanosensitive Channel. *Biophys. J* **2011**, *100*, 1651–1659.

(7) Rzepiela, A. J.; Schäfer, L. V.; Goga, N.; Risselada, H. J.; de Vries, A. H.; Marrink, S. J. Reconstruction of Atomistic Details from Coarse Grained Structures. *J. Comp. Chem.* **2010**, *31*, 1333–1343.

(8) Kandt, C.; Ash, W. L.; Tieleman, D. P. Setting Up and Running Molecular Dynamics Simulations of Membrane Proteins. *Methods* **2007**, *41*, 475–488.

(9) Miyamoto, S.; Kollman, P. A. SETTLE: an Analytical Version of the SHAKE and RATTLE Algorithms for Rigid water Models. *J. Comput. Chem.* **1992**, *13*, 952–962.

(10) Hess, B.; Bekker, H.; Berendsen, H. J. C.; Fraaije, J. G. E. M. LINCS: a Linear Constraint Solver for Molecular Simulations. *J. Comput. Chem.* **1998**, *18*, 1463–1472.

(11) Darden, T.; York, D.; Pedersen, L. Particle Mesh Ewald: an N-log(N) Method for Ewald Sums in Large Systems. *J. Chem. Phys.* **1993**, *98*, 10089–10092.

(12) Nos*é*, S. A Molecular Dynamics Method for Simulations in the Canonical Ensemble. *Mol. Phys.* **1984**, *52*, 255–268.

(13) Hoover, W. G. Canonical Dynamics: Equilibrium Phase-Space Distributions. *Phys. Rev. A* **1985**, *31*, 1695–1697.

(14) Parrinello, M.; Rahman, A. Polymorphic Transitions in Single Crystals: A New Molecular Dynamics Method. *J. Appl. Phys.* **1981**, *52*, 7182–7190.

(15) Jansen, T. L. C.; Dijkstra, A. G.; Watson, T. M.; Hirst, J. D.; Knoester, J. Modeling the Amide I Bands of Small Peptides. *J. Chem. Phys.* **2006**, *125*, 44312.

(16) Jansen, T. L. C.; Knoester, J. A Transferable Electrostatic Map for Solvation Effects on Amide I Vibrations and its Application to Linear and Two-Dimensional Spectroscopy. *J. Chem. Phys.* **2006**, *124*, 044502.

(17) Roy, S.; Lessing, J.; Meisl, G.; Ganim, Z.; Tokmakoff, A.; Knoester, J.; Jansen, T. L. C. Solvent and Conformation Dependence of Amide I Vibrations in Peptides and Proteins Containing Proline. *J. Chem. Phys* **2011**, *135*, 234507.

(18) Wang, L.; Middelton, C. T.; Zanni, M. T.; Skinner, J. L. Development and Validation of Transferable Amide I Vibrational Frequency Maps for Peptides. *J. Phys. Chem. B* **2011**, *115*, 3713–3724.

(19) Lessing, J.; Roy, S.; Reppert, M.; Baer, M. D.; Marx, D.; Jansen, T. l. C.; Knoester, J.; Tokmakoff, A. Identifying Residual Structure in Intrinsically Disordered Systems: A 2D IR Spectroscopic Study of the GVGXPGVG Peptide. *J. Am. Chem. Soc.* **2012**, *134*, 5032–5035.

(20) Woys, A. M.; Almeida, A. M.; Wang, L.; Chiu, C.-C.; McGovern, M.; de Pablo, J. J.; Skinner, J. L.; Gellman, S. H.; Zanni, M. T. Parallel $\beta$-sheet Vibrational Couplings Revealed by 2D IR Spectroscopy of an Isotopically Labeled Macrocycle: Quantitative Benchmark for the Interpretation of Amyloid and Protein Infrared Spectra . *J. Am. Chem. Soc.* **2012**, *134*, 19118–19128.

(21) Hochstrasser, R. M. Two-dimensional IR-spectroscopy: Polarization Anisotropy Effects. *Chem. Phys.* **2001**, *266*, 273–284.

(22) Löbau, J.; Wolfrum, K. Sum-Frequency Spectroscopy in Total Internal Reflection Geometry: Signal Enhancement and Access to Molecular Properties. *J. Opt. Soc. Am. B* **1997**, *14*, 2505–2512.

(23) Ji, N.; Ostroverkhov, V.; Tian, C. S.; Shen, Y. R. Characterization of Vibrational Resonances of Water-Vapor Interfaces by Phase-Sensitive Sum-Frequency Spectroscopy. *Phys. Rev. Lett.* **2008**, *100*, 096102.

(24) Tian, C. S.; Shen, Y. R. Structure and Charging of Hydrophobic Material/Water Interfaces Studied by Phase-Sensitive Sum-Frequency Vibrational Spectroscopy. *Proc. Natl. Acad. Sci. USA* **2009**, *106*, 15148–15153.

(25) Nguyen, K. T.; le Clair, S. V.; Ye, S.; Chen, Z. Orientation Determination of Protein Helical Secondary Structures using Linear and Nonlinear Vibrational Spectroscopy. *J. Phys. Chem. B* **2009**, *113*, 12169–12180.

(26) Nguyen, K. T.; King, J. T.; Chen, Z. Orientation Determination of Interfacial $\beta$-sheet Structures in Situ. *J. Phys. Chem. B* **2010**, *114*, 8291–8300.

(27) Tsuboi, M.; Thomas, G. J. Raman Scattering Tensors in Biological Molecules and Their Assemblies. *Appl. Spectro. Rev.* **1997**, *32*, 263–299.

(28) Jansen, T. L. C.; Knoester, J. Nonadiabatic Effects in the Two-Dimensional Infrared Spectra of Peptides: Application to Alanine Dipeptide. *J. Phys. Chem. B* **2006**, *110*, 22910–22916.

(29) Lin, Y. S.; Shorb, J. M.; Mukherjee, P.; Zanni, M. T.; Skinner, J. L. Empirical Amide I Vibrational Frequency Map: Application to 2D-IR Line Shapes for Isotope-Edited Membrane Peptide Bundles. *J. Phys. Chem. B* **2009**, *113*, 592–602.

(30) Grechko, M.; Zanni, M. T. Quantification of Transition Dipole Strengths using 1D and 2D Spectroscopy for the Identification of Molecular Structures via Exciton Delocalization: Application to $\alpha$-helices. *J. Chem. Phys.* **2012**, *137*, 184202.

(31) Chung, H. S.; Ganim, Z.; Jones, K. C.; Tokmakoff, A. Transient 2D IR Spectroscopy of Ubiquitin Unfolding Dynamics. *P. Nat. Acad. Sci.* **2007**, *104*, 14237.

(32) Cheatum, C. M.; Tokmakoff, A.; Knoester, J. Signatures of Beta-sheet Secondary Structures in Linear and Two-Dimensional Infrared Spectroscopy. *J. Chem. Phys.* **2004**, *120*, 8201.

(33) Woutersen, S.; Hamm, P. Time-resolved Two-Dimensional Vibrational Spectroscopy of a Short Alpha-helix in Water. *J. Chem. Phys.* **2001**, *115*, 7737.

(34) Jansen, T. L. C.; Knoester, J. Two-Dimensional Infrared Population Transfer Spectroscopy for Enhancing Structural Markers of Proteins. *Biophys. J.* **2008**, *94*, 1818–1825.

(35) Karjalainen, E.-L.; Barth, A. Vibrational Coupling between Helices Influences the Amide I Infrared Absorption of Proteins: Application to Bacteriorhodopsin and Rhodopsin. *J. Phys. Chem. B* **2012**, *116*, 4448–4456.

**Table S1: The tilt angles $\theta_{helix}$ of transmembrane helices TM1 and TM2.**

| $\theta_{helix}$ | closed | inter | open |
|---|---|---|---|
| TM1 | 52° | 53° | 74° |
| TM2 | 34° | 42° | 52° |

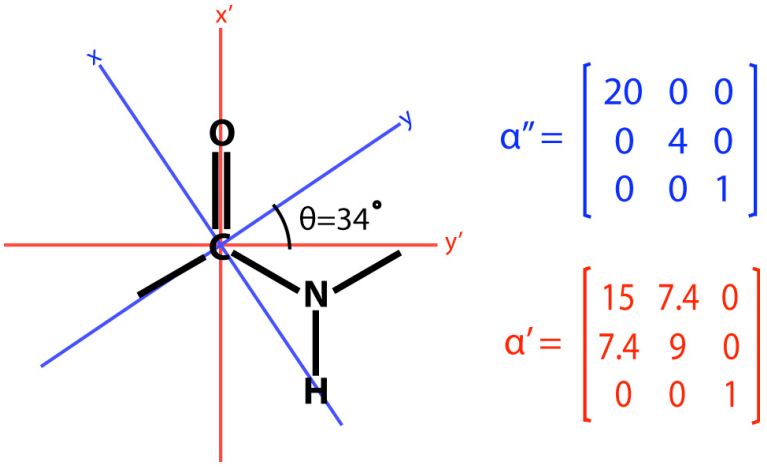


Figure S1: Schematic figure of the peptide group in different molecular frames, and the corresponding polarization Raman tensors.

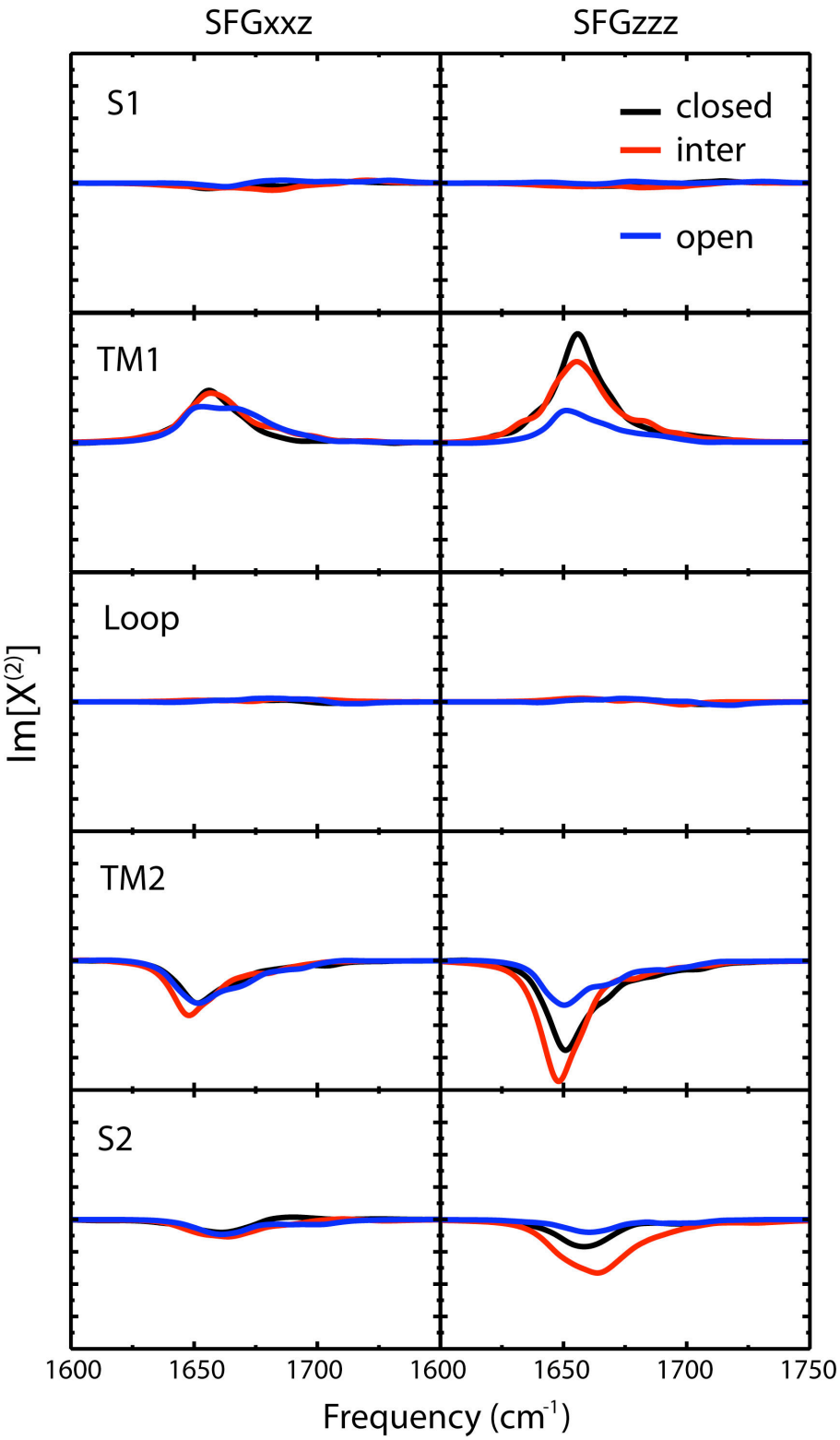


Figure S2: SFG response functions of different groups. The scaling of the signal intensities is preserved in all panels so the signals give an indication of the relative contributions to the total signal.

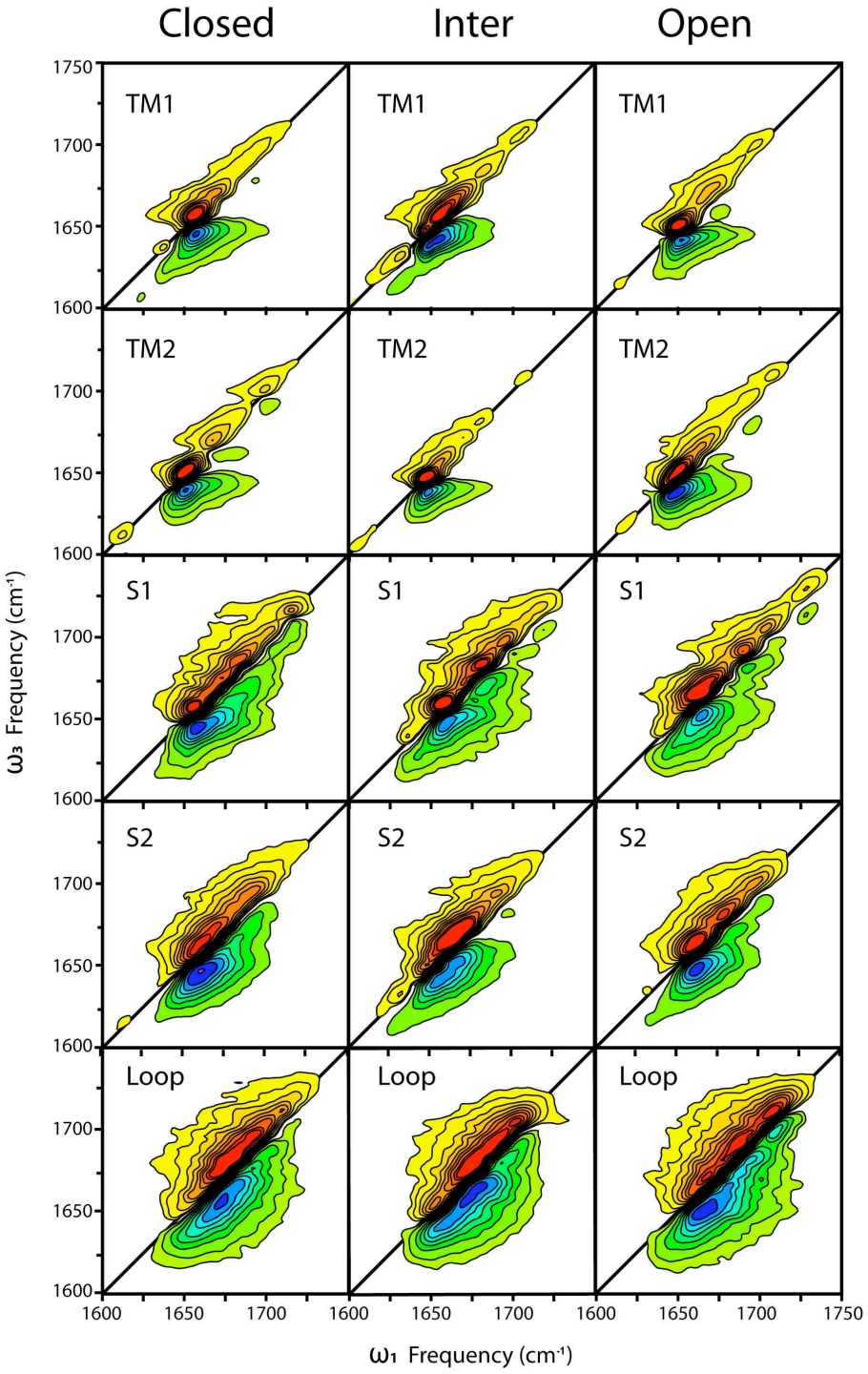


Figure S3: The parallel polarization 2DIR spectra of different groups. 2DIR spectra are normalized to the maximal intensity amplitude, and each color contour represents 10% of the maximal amplitude.

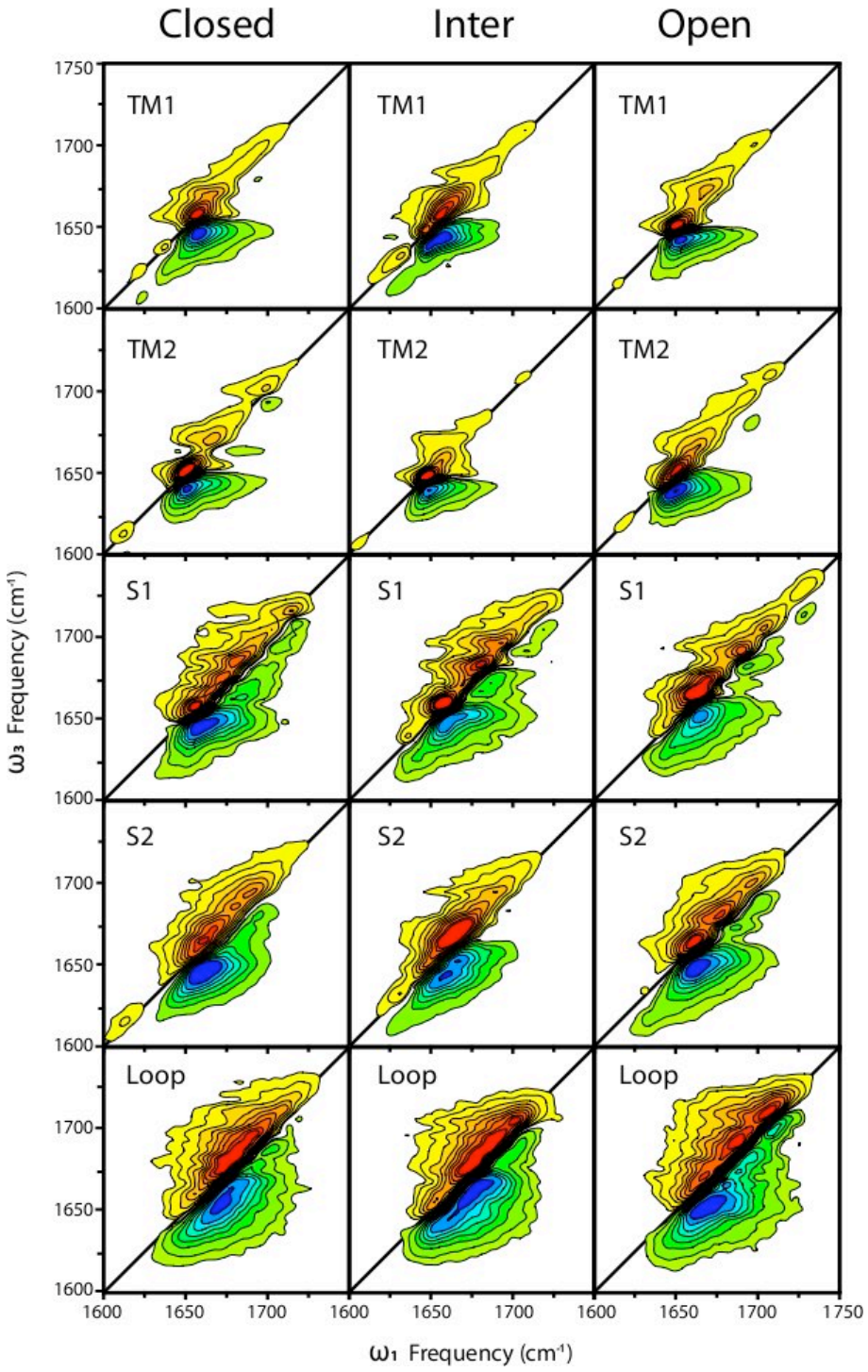


Figure S4: The perpendicular polarization 2DIR spectra of different groups. 2DIR spectra are normalized to the maximal intensity amplitude, and each color contour represents 10% of the maximal amplitude.

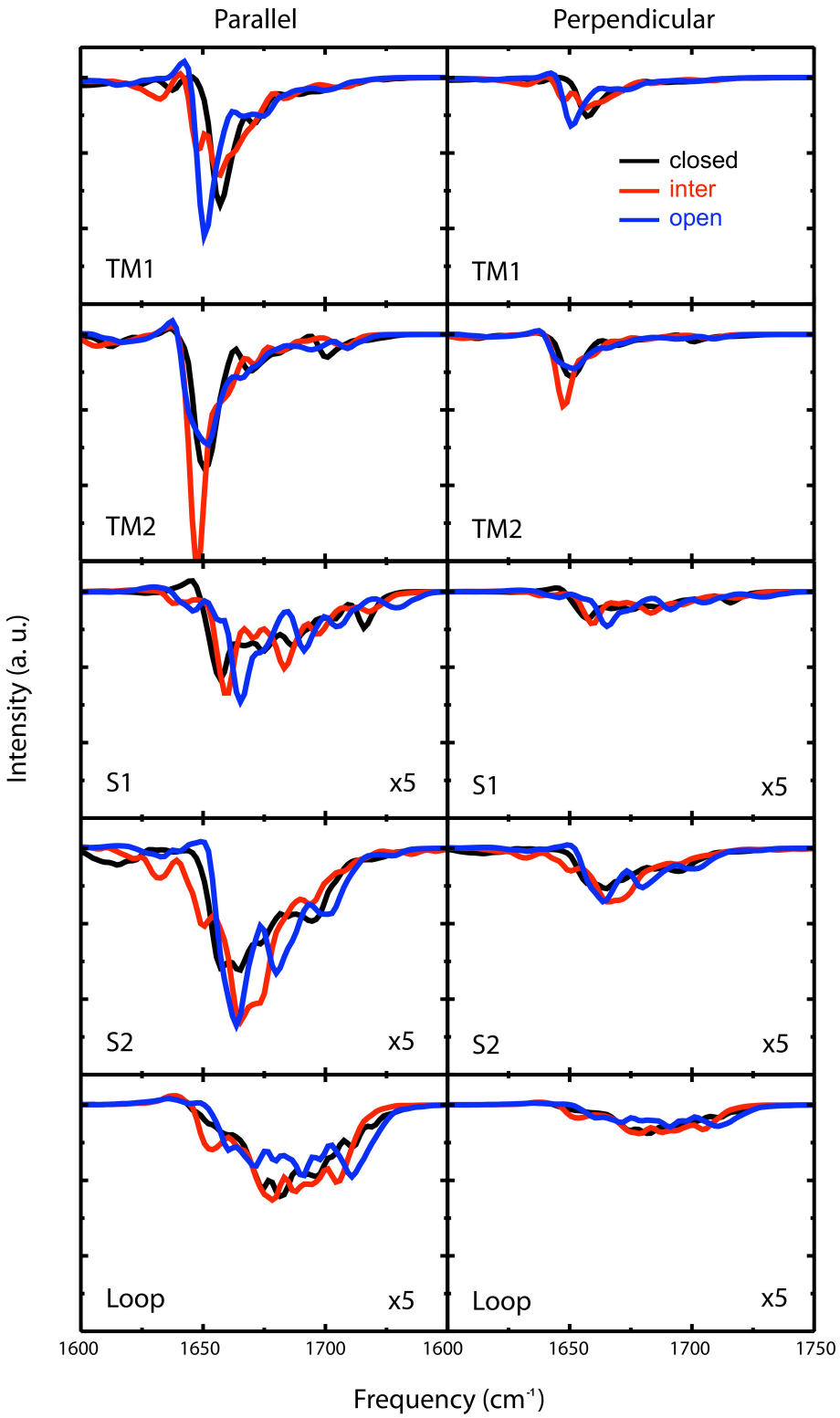


Figure S5: Diagonal slices through the 2DIR spectra presented in Figure S3 and S4. The signals for S1, S2, and the loop are magnified with a factor 5 for clarity.